

Periodically multilayered planar optical concentrator for photovoltaic solar cells

Manuel E. Solano, Muhammad Faryad, Peter B. Monk, Thomas E. Mallouk, and Akhlesh Lakhtakia

Citation: [Applied Physics Letters](#) **103**, 191115 (2013); doi: 10.1063/1.4829641

View online: <http://dx.doi.org/10.1063/1.4829641>

View Table of Contents: <http://scitation.aip.org/content/aip/journal/apl/103/19?ver=pdfcov>

Published by the [AIP Publishing](#)

Articles you may be interested in

[Low-loss waveguiding and detecting structure for surface plasmon polaritons](#)

Appl. Phys. Lett. **104**, 081111 (2014); 10.1063/1.4866792

[Direct generation of charge carriers in c-Si solar cells due to embedded nanoparticles](#)

J. Appl. Phys. **102**, 093713 (2007); 10.1063/1.2809368

[Surface plasmon enhanced silicon solar cells](#)

J. Appl. Phys. **101**, 093105 (2007); 10.1063/1.2734885

[Improved performance of amorphous silicon solar cells via scattering from surface plasmon polaritons in nearby metallic nanoparticles](#)

Appl. Phys. Lett. **89**, 093103 (2006); 10.1063/1.2336629

[Periodic light coupler gratings in amorphous thin film solar cells](#)

J. Appl. Phys. **89**, 7722 (2001); 10.1063/1.1370996

The advertisement features a row of computer monitors in a library setting, each displaying the cover of the journal 'Computing in Science & Engineering'. The covers show colorful, abstract patterns. In the bottom right corner, the journal's logo is displayed in orange and black. Below the monitors, the text 'AIP's JOURNAL OF COMPUTATIONAL TOOLS AND METHODS. AVAILABLE AT MOST LIBRARIES.' is written in white and yellow on a dark background.

computing
IN SCIENCE & ENGINEERING

AIP's JOURNAL OF COMPUTATIONAL TOOLS AND METHODS.
AVAILABLE AT MOST LIBRARIES.

Periodically multilayered planar optical concentrator for photovoltaic solar cells

Manuel E. Solano,¹ Muhammad Faryad,² Peter B. Monk,¹ Thomas E. Mallouk,³ and Akhlesh Lakhtakia^{2,a)}

¹Department of Mathematical Sciences, University of Delaware, Newark, Delaware 19716, USA

²Department of Engineering Science and Mechanics, Pennsylvania State University, University Park, Pennsylvania 16802, USA

³Department of Chemistry, Pennsylvania State University, University Park, Pennsylvania 16802, USA

(Received 27 September 2013; accepted 26 October 2013; published online 7 November 2013)

A planar optical concentrator comprising a periodic multilayered isotropic dielectric material backed by a metallic surface-relief grating was theoretically examined for silicon photovoltaics. The concentrator was optimized using a differential evolution algorithm for solar-spectrum-integrated power-flux density. Further optimization was carried out for tolerance to variations in the incidence angle, spatial dimensions, and dielectric properties. The average electron-hole pair density in a silicon solar cell can be doubled, and the material costs substantially diminished by this concentrator, whose efficacy is due to the excitation of waveguide modes and multiple surface-plasmon-polariton waves in a broad spectral regime. © 2013 AIP Publishing LLC. [<http://dx.doi.org/10.1063/1.4829641>]

A planar optical concentrator (POC) is a laminar structure with solar cells mounted on its edges. Solar radiation falling on the POC is redirected to travel along the sheet towards the solar cells. While early work on these concentrators focused on device designs with large areas and high concentration ratios,¹⁻³ recent advances in soft lithography and particle assembly have made it possible to inexpensively fabricate arrays of microscopic solar cells over large areas.⁴⁻⁶ These patterning techniques now allow module designs in which light is guided over millimeter or even shorter distances. Such designs are more tolerant of lossy materials, such as luminescent dyes or plasmonic metal gratings. They are also amenable to relatively low concentration ratios, which are appropriate for absorber materials of moderate cost such as single-crystal silicon.

In this letter, we propose a low-concentration-ratio POC comprising a periodic multi-layered isotropic dielectric (PMLID) material backed by a metallic surface-relief grating. This concentrator is inspired by recent theoretical⁷ and experimental⁸ results showing that the interface of a metal and a PMLID material can guide multiple surface-plasmon-polariton waves having different polarization states, phase speeds, propagation lengths, and spatial field profiles but of the same frequency and direction of propagation.⁹

One unit cell of a structure comprising the proposed POC and a solar cell is shown schematically in Fig. 1. The structure occupies the region $0 < z < L_t = L_d + L_g + L_m$. The region $z > L_t$ is vacuous. Except for a 100-nm-thick layer of indium tin oxide atop the structure, the region $z < 0$ is also vacuous. The reference unit cell is the region $\{0 < x < (N_c + N_s)L, 0 < z < L_t\}$. The solar cell is made of crystalline silicon and is backed by the same grating.

The PMLID material occupies the region $\{0 < x < N_c L, 0 < z < L_d\}$ in the reference unit cell. Each period of the PMLID material comprises N layers, where the width and

the relative permittivity of the j th layer, $j \in [1, N]$, are denoted by d_j and ϵ_{rj} , respectively; $\sum_{j=1}^N d_j = 2\Omega$. The region $\{0 < x < N_c L, L_d < z < L_t\}$ is occupied by a metallic surface-relief grating with its troughs filled by a dielectric material of relative permittivity ϵ_{r1} . The metal/dielectric surface has a periodic rectangular profile with a period L along the x axis, corrugation height L_g , and duty cycle $\zeta = L_1/L$. The relative permittivity of the metal is denoted by ϵ_m , $\text{Re}[\epsilon_m] < 0$. Crystalline silicon occupies the region $\{N_c L < x < (N_c + N_s)L, 0 < z < L_d\}$ in the reference unit cell. The region $\{N_c L < x < (N_c + N_s)L, L_d < z < L_t\}$ is occupied by the metallic surface-relief grating with its troughs filled by crystalline silicon. All relative permittivities are functions of the free-space wavelength λ_0 .

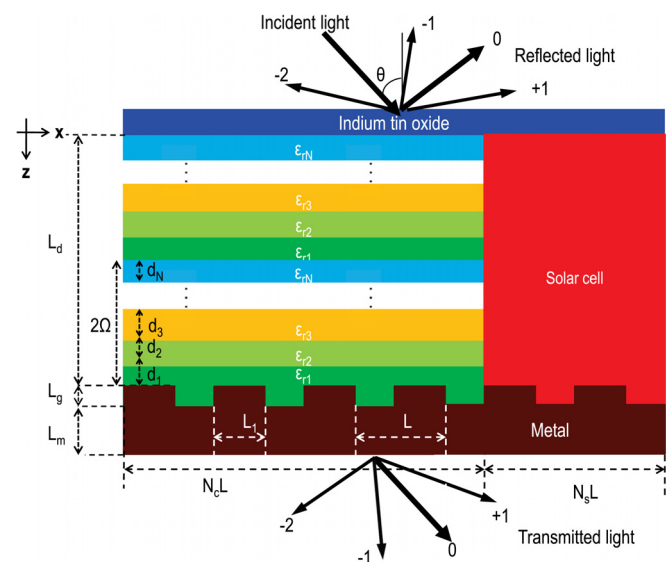


FIG. 1. Schematic of the reference unit cell of the proposed structure. When a plane wave is incident, the reflected and the transmitted fields comprise specular components (labeled 0) and nonspecular components (labeled $\pm 1, \pm 2, \dots$).

^{a)}Electronic mail: akhlesh@psu.edu

The efficacy of the structure was investigated in two steps. In the first step, the solar cell and the indium-tin-oxide layer were absent, and the concentrator was optimized to maximize the solar-spectrum-integrated power-flux density (in $\text{W}^2 \text{m}^{-2}$)

$$q(x) = \int_{\lambda_{0\min}}^{\lambda_{0\max}} \lambda_0 S(\lambda_0) \left[\int_0^{L_d} |P_x(x, z; \lambda_0)| dz \right] d\lambda_0, \quad (1)$$

when an unpolarized plane wave (with an electric field of amplitude of $E_o = 1 \text{ V m}^{-1}$) is incident on the structure with its wave vector oriented in the xz plane and directed at angle θ with respect to the z axis. Here, $P_x(x, z; \lambda_0)$ is the x -directed component of the monochromatic time-averaged Poynting vector $\mathbf{P}(x, z; \lambda_0)$, $S(\lambda_0)$ is the AM1.5 solar spectrum, $\lambda_{0\min} = 400 \text{ nm}$, and $\lambda_{0\max} = 1000 \text{ nm}$. The rigorous coupled-wave approach (RCWA)^{10,11} was used to calculate $\mathbf{P}(x, z; \lambda_0)$. In the second step, the optimized concentrator was used with the solar cell and the indium-tin-oxide layer, and the average current density in the solar cell was calculated using the finite element method (FEM).¹²

The differential evolution algorithm^{13,14} is suitable for optimization when the cost function is non-differentiable, multidimensional, and/or several local maximums. Hence, this algorithm is attractive for optimizing the stand-alone concentrator. As a metaheuristic algorithm that iteratively improves the candidate solution based on random movements in the search space, this algorithm does not require evaluations of the gradients of the cost function. This is also advantageous in the present context.

The metal was chosen to be silver, and $L_m = 40 \text{ nm}$ was fixed. The unit cell of the PMLID material was taken to comprise $N = 9$ distinct layers of the same thickness (i.e., $d_j = d \forall j \in [1, N]$). However, their dielectric properties were all different, per $\epsilon_{rj} = [(1 + \delta)(A_j + B_j \lambda_0^{-2} + C_j \lambda_0^{-4})]^2$, $j \in [1, N]$, with $\delta \in [-0.25, 0.25]$ and measured coefficients $\{A_j, B_j, C_j\}$ available for silicon oxynitrides of diverse compositions.⁷ The PMLID material was taken to have 3 periods, i.e., $L_d = 6\Omega$. For numerically implementing the RCWA, 17 terms were used in Fourier expansions of the relative permittivity (in the region $L_d < z < L_d + L_g$) and the field phasors with respect to x for s -polarized incidence for $\lambda_0 \in [400, 1100] \text{ nm}$ after verifying the convergence of \mathbf{P} ; for

p -polarized incidence, 17 terms were used when $\lambda_0 \leq 500 \text{ nm}$ and 29 terms were used when $\lambda_0 > 500 \text{ nm}$. The mean value of $|P_x|$ for both linear polarization states was used in Eq. (1).

Calculated values of $q(x)$ for $x \in \{0, L/2, 3L/2\}$ are presented in Table I when $L = 400 \text{ nm}$, $d = 80 \text{ nm}$, and $\delta = 0$ were fixed, but $L_g \in \{40, 60, 80\} \text{ nm}$, $\zeta \in \{0.3, 0.5, 0.7\}$, and $\theta \in \{15^\circ, 30^\circ\}$ were kept variable. Although $q(x)$ definitely depends on x , the table shows that the choice of x is immaterial for the determination of the optimal values of the triad $\{L_g, \theta, \zeta\}$. Accordingly, we chose $q(0)$ for optimizing the concentrator using the differential evolution algorithm.

Next, the search space for the differential evolution algorithm was chosen after inspection of several other numerical results obtained using the RCWA. Thus, optimal parameters were searched on the following intervals: $\theta \in [0^\circ, 45^\circ]$, $d \in [40, 100] \text{ nm}$, $\delta \in [-0.25, 0.25]$, $\zeta \in (0, 1)$, and $L_g \in [30, 100] \text{ nm}$. The differential evolution algorithm was allowed to run for 300 cycles. For a fixed period $L = 400 \text{ nm}$, the maximum of $q(0)$ was found to be $1.17 \times 10^{-10} \text{ W}^2 \text{m}^{-2}$ for the following set of optimal values: $\theta = 6^\circ$, $d = 105 \text{ nm}$, $\delta = -0.02$, $\zeta = 0.3$, and $L_g = 42 \text{ nm}$.

In order to delineate the different spectral contributions to $q(0)$, plots of $|P_x(0, z; \lambda_0)|$ are provided in Fig. 2 for (a) the optimal case and (b) a sub-optimal case with $\theta = 20^\circ$, $d = 50 \text{ nm}$, $\delta = -0.25$, $\zeta = 0.5$, and $L_g = 30 \text{ nm}$. Several high- $|P_x|$ bands are present for the optimal case when $\lambda_0 \in (400, 700) \text{ nm}$. In contrast, only a few such bands exist—that too of reduced magnitudes—for the sub-optimal case.

The high- $|P_x|$ bands are due to the excitation of either waveguide modes traveling in the bulk of the PMLID material or surface-plasmon-polariton waves guided by the metal/PMLID interface.⁷ This was established from the plots of $|E_y(x, z; \lambda_0)|^2$ presented in Fig. 3 for the optimal case when λ_0 is either (a) 624 nm or (b) 625 nm for s -polarized incidence. Figure 3(a) indicates the presence of an s -polarized waveguide mode because the energy is primarily distributed throughout the PMLID material and is not localized to the metal/PMLID interface. In Fig. 3(b), drawn for $\lambda_0 = 625 \text{ nm}$, the presence of an s -polarized surface-plasmon-polariton wave is clear because the electric field is localized to the metal/PMLID interface; confirmation was also obtained by solving an underlying canonical problem.⁷

TABLE I. Calculated values of $q(x)$ (normalized by $10^{-12} \text{ W}^2 \text{m}^{-2}$) for $x \in \{0, L/2, 3L/2\}$ in the reference unit cell, when $L = 400 \text{ nm}$, $d = 80 \text{ nm}$, $N = 9$, and $\delta = 0$. The bold values were found to be the optimal for the chosen parameters.

θ	L_g (nm)	$x = 0$			$x = L/2$			$x = 3L/2$		
		$\zeta = 0.3$	$\zeta = 0.5$	$\zeta = 0.7$	$\zeta = 0.3$	$\zeta = 0.5$	$\zeta = 0.7$	$\zeta = 0.3$	$\zeta = 0.5$	$\zeta = 0.7$
15°	40	1.22	1.76	1.18	1.23	1.78	1.20	1.13	1.68	1.12
	60	1.56	1.65	1.47	1.59	1.67	1.48	1.47	1.57	1.40
	80	1.69	1.59	1.61	1.72	1.62	1.63	1.60	1.51	1.53
30°	40	1.33	1.40	1.95	1.35	1.43	1.96	1.30	1.38	1.92
	60	5.68	1.63	1.85	5.71	1.66	1.86	5.64	1.59	1.82
	80	2.37	2.39	1.85	2.38	2.40	1.86	2.31	2.33	1.81
45°	40	1.19	1.00	1.08	1.21	1.02	1.09	1.19	0.99	1.07
	60	1.94	1.22	1.07	1.96	1.24	1.08	1.93	1.21	1.06
	80	1.25	1.26	1.07	1.27	1.27	1.08	1.43	1.24	1.06

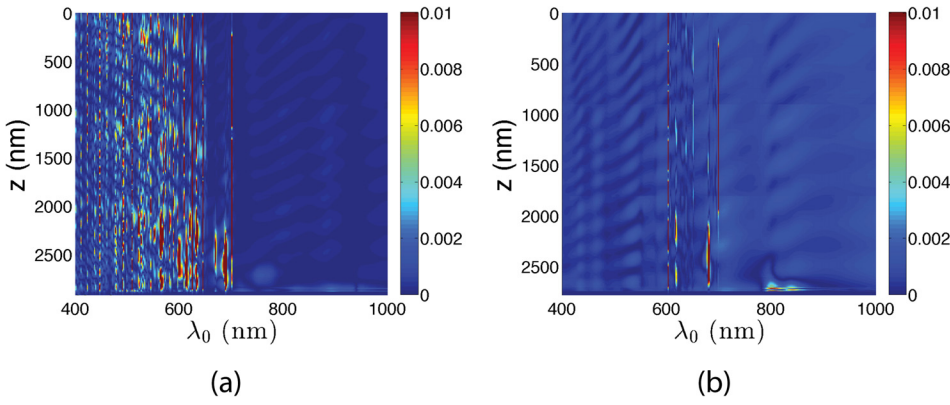


FIG. 2. Variation of $|P_x(0, z; \lambda_0)|$ (in W m^{-2}) with z and λ_0 for the stand-alone concentrator with $L = 400$ nm. (a) Optimal case: $\theta = 6^\circ$, $d = 105$ nm, $\delta = -0.02$, $\zeta = 0.3$, and $L_g = 42$ nm. (b) A sub-optimal case: $\theta = 20^\circ$, $d = 50$ nm, $\delta = -0.25$, $\zeta = 0.5$, and $L_g = 30$ nm.

Let us now consider the complete structure shown schematically in Fig. 1. Both N_c and N_s are variables. For an unpolarized incident plane wave with an electric field of magnitude $E_o = 1 \text{ V m}^{-1}$, the electric field $\mathbf{E}(x, z; \lambda_0)$ in the reference unit cell was computed using the FEM.¹² The switchover from the RCWA to the FEM was necessitated by the prohibitively large number of terms needed in the Fourier expansions of the field phasors with respect to x in RCWA when the overall period $(N_c + N_s)L$ becomes very large in relation to λ_0 .¹⁵ The FEM mesh was designed so that each element was completely contained in a homogeneous material; the field phasors were represented by cubic polynomials in each element; the mesh size was about $L/4$; quasi-periodic boundary conditions were imposed on the two ends of the interval $0 < x < (N_c + N_s)L$; the boundary conditions on the top face of the indium-tin-oxide layer and the

plane $z = L_t$ were implemented via a Lagrange multiplier; and the incident, reflected, and transmitted fields were represented as spectrums of $2M + 1$ plane waves, with M is the smallest integer $\geq 1.2(N_c + N_s)$.

Thereafter, the average electron-hole pair (EHP) density was computed as

$$N_{avg}^{(N_c, N_s)} = \int_{\lambda_{0min}}^{\lambda_{0max}} \left(\lambda_0 \frac{S(\lambda_0) \text{Im}[\epsilon_{rs}(\lambda_0)]}{N_s L L_d c_0 \hbar E_o^2 \cos \theta} \times \left\{ \int_{x=N_c L}^{(N_c + N_s)L} \left[\int_{z=0}^{L_d} |\mathbf{E}(x, z; \lambda_0)|^2 dz \right] dx \right\} \right) d\lambda_0, \quad (2)$$

where c_0 is the speed of light in free space, \hbar is the reduced Planck constant, and $\epsilon_{rs}(\lambda_0)$ is the relative permittivity of crystalline silicon. All calculations were made for $\theta = 6^\circ$, $d = 105$ nm, $\delta = -0.02$, $\zeta = 0.3$, $L_g = 42$ nm, and $L = 400$ nm, with N_c and N_s kept variable.

Table II presents $N_{avg}^{(N_c, 1)}$ in relation to N_c . Clearly, the average EHP density doubles when $N_c = 2$ in comparison to the situation when the concentrator is absent. However, the incremental rise $1 - (N_{avg}^{(N_c-1, 1)}/N_{avg}^{(N_c, 1)})$ decreases to less than 5% for $N_c \leq 4$. This result suggests that the technologically optimal value of the ratio N_c/N_s is likely to be small although the economically optimal value of that ratio may be somewhat higher because the dielectric layers can be considerably less expensive than crystalline silicon.

TABLE II. Calculated values of $N_{avg}^{(N_c, 1)}$, $1 - (N_{avg}^{(N_c-1, 1)}/N_{avg}^{(N_c, 1)})$, and $N_{avg}^{(N_c, 1)}/N_{avg}^{(0, 1)}$ vs. N_c for the optimal case: $\theta = 6^\circ$, $d = 105$ nm, $\delta = -0.02$, $\zeta = 0.3$, $L_g = 42$ nm, and $L = 400$ nm.

N_c	$N_{avg}^{(N_c, 1)}$ (cm^{-2})	$1 - (N_{avg}^{(N_c-1, 1)}/N_{avg}^{(N_c, 1)})$	$N_{avg}^{(N_c, 1)}/N_{avg}^{(0, 1)}$
0	7.1749×10^{15}	...	1.00
1	1.2516×10^{16}	0.74	1.74
2	1.4567×10^{16}	0.16	2.03
3	1.5452×10^{16}	0.06	2.15
4	1.6088×10^{16}	0.04	2.24
5	1.6677×10^{16}	0.03	2.31
6	1.7482×10^{16}	0.05	2.42
7	1.8014×10^{16}	0.03	2.50
8	1.8804×10^{16}	0.04	2.61
9	1.9537×10^{16}	0.04	2.71
10	1.9804×10^{16}	0.01	2.75

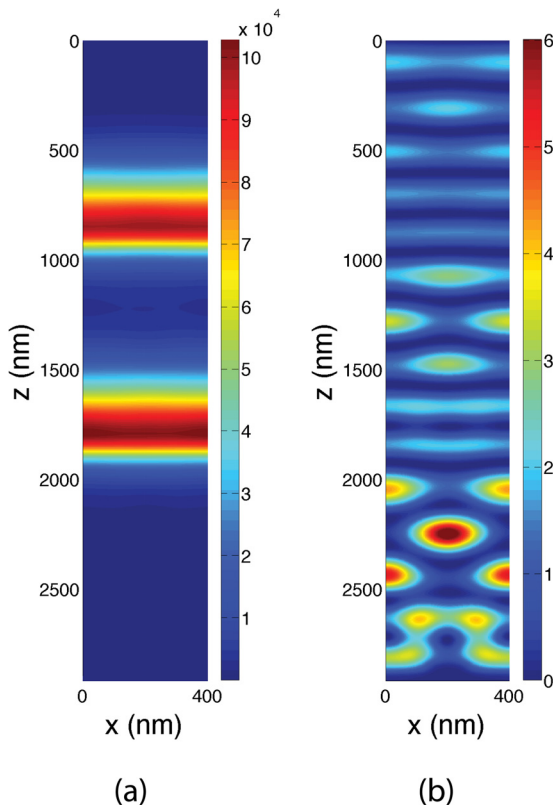
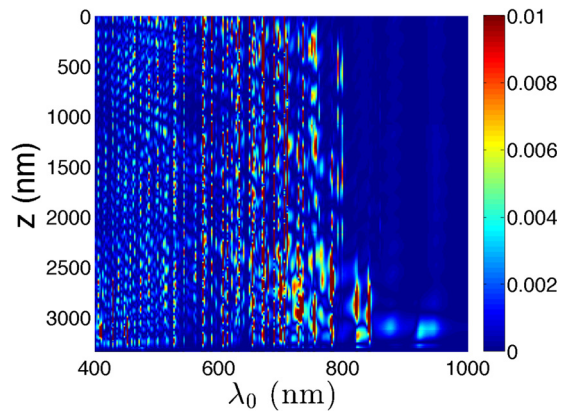


FIG. 3. Variation of $|E_y(x, z; \lambda_0)|^2$ (in $\text{V}^2 \text{m}^{-2}$) with x and z for the optimal structure described for Fig. 2(a). The incident plane wave is s polarized. (a) $\lambda_0 = 624$ nm. (b) $\lambda_0 = 625$ nm.

TABLE III. Calculated values of $N_{avg}^{(N_c,2)}$ and $N_{avg}^{(N_c,3)}$ vs. N_c for the same parameters as in Table II.

$N_s = 2$		$N_s = 3$	
N_c	$N_{avg}^{(N_c,2)}$ (cm^{-2})	N_c	$N_{avg}^{(N_c,3)}$ (cm^{-2})
2	1.1971×10^{16}	3	1.1067×10^{16}
4	1.2757×10^{16}	6	1.1871×10^{16}
6	1.3527×10^{16}	9	1.2651×10^{16}
8	1.4285×10^{16}	12	1.3357×10^{16}

FIG. 4. Same as Fig. 2(a) except that $\theta = 7^\circ$, $d = 120$ nm, $\delta = 0.2$, $\zeta = 0.72$, and $L_g = 62$ nm.

Increasing N_s from 1 while keeping N_c fixed somewhat decreases the average EHP density. This is deduced from a comparison of $N_{avg}^{(N_c,1)}$ (Table II) with $N_{avg}^{(N_c,2)}$ and $N_{avg}^{(N_c,3)}$ provided in Table III.

The optimized concentrator (with parameters the same as for Figs. 2(a) and 3 and for Tables II and III) is very sensitive to small changes in its parameters. In order to overcome manufacturing challenges to deliver high precision, we re-optimized the design so that a variation of up to 5% in a parameter does not result in change in $q(0)$ by more than 10%. Running 300 iterations of the differential evolution algorithm, we found a concentrator suitable for practical implementation with $q(0) = 4.74 \times 10^{-12} \text{ W}^2 \text{ m}^{-2}$ when $\theta = 7^\circ$, $d = 120$ nm, $\delta = 0.2$, $\zeta = 0.72$, $L_g = 62$ nm, and $L = 400$ nm.

The plot of $|P_x(0, z; \lambda_0)|$ as a function of λ_0 and z in Fig. 4 for the practically implementable concentrator does not have sharp peaks as in Fig. 2(a) but provides evidence that waveguide modes¹⁶ and surface-plasmon-polariton waves¹⁷ shall be excited over a larger spectral regime as compared to Fig. 2(a). From the data on $N_{avg}^{(N_c,1)}$ in relation to N_c in Table IV, it follows that the average EHP density is almost the same as for the optimal case (Table II). Moreover, increasing N_s while keeping N_c fixed remains detrimental to the average EHP density. Thus, the practically implementable concentrator will not exhibit a reduction of the average EHP density even though it is more tolerant to variations in the angle of incidence, spatial

TABLE IV. Same as in Table II except $\theta = 7^\circ$, $d = 120$ nm, $\delta = 0.2$, $\zeta = 0.72$, and $L_g = 62$ nm.

N_c	$N_{avg}^{(N_c,1)}$ (cm^{-2})	$1 - (N_{avg}^{(N_c,1)}/N_{avg}^{(N_c,1)})$	$N_{avg}^{(N_c,1)}/N_{avg}^{(0,1)}$
0	6.7234×10^{15}	...	1.00
1	1.1891×10^{16}	0.77	1.77
2	1.3852×10^{16}	0.16	2.06
3	1.4801×10^{16}	0.07	2.20
4	1.5581×10^{16}	0.05	2.32
5	1.6444×10^{16}	0.06	2.44
6	1.7244×10^{16}	0.05	2.56
7	1.8032×10^{16}	0.05	2.68
8	1.8827×10^{16}	0.04	2.80
9	1.9326×10^{16}	0.03	2.87
10	1.9653×10^{16}	0.02	2.92

dimensions, and dielectric properties than the optimized concentrator.

The periodically multilayered POC proposed in this letter can be used to replace a significant fraction of silicon by cheaper (although not photovoltaic) materials and could therefore reduce the cost of solar cells without a concomitant reduction in efficiency. For instance, the replacement of two-thirds of a solar cell by the concentrator results in about 33% reduction of the average EHP density, as is indicated by the results for $N_c = 2$ in Table IV, but that reduction could be compensated by a reduction in material costs.

This work was supported by the National Science Foundation under Grant No. DMR-1125591.

- ¹W. H. Weber and J. Lambe, *Appl. Opt.* **15**, 2299 (1976); J. S. Batchelder, A. H. Zewail, and T. Cole, *ibid.* **18**, 3090 (1979).
- ²R. W. Olson, R. Loring, and M. D. Fayer, *Appl. Opt.* **20**, 2935 (1981).
- ³M. J. Currie, J. K. Mapel, T. D. Heidel, S. Goffrie, and M. A. Baldo, *Science* **321**, 226 (2008).
- ⁴J. Yoon, A. J. Baca, S.-I. Park, P. Elvikis, J. B. Geddes, L. Li, R. H. Kim, J. Xiao, S. Wang, T. H. Kim, M. J. Motala, B. Y. Ahn, E. B. Duoss, J. A. Lewis, R. G. Nuzzo, P. M. Ferreira, Y. Huang, A. Rockett, and J. A. Rogers, *Nature Mater.* **7**, 907 (2008).
- ⁵J. Yoon, L. F. Li, A. V. Semichaevsky, J. H. Ryu, H. T. Johnson, R. G. Nuzzo, and J. A. Rogers, *Nature Comm.* **2**, 343 (2011).
- ⁶R. J. Knuesel and H. O. Jacobs, *Adv. Mater.* **23**, 2727 (2011).
- ⁷M. Faryad, A. S. Hall, G. D. Barber, T. E. Mallouk, and A. Lakhtakia, *J. Opt. Soc. Am. B* **29**, 704 (2012).
- ⁸A. S. Hall, M. Faryad, G. D. Barber, L. Liu, S. Erten, T. S. Mayer, A. Lakhtakia, and T. E. Mallouk, *ACS Nano* **7**, 4995 (2013).
- ⁹J. A. Polo, Jr., T. G. Mackay, and A. Lakhtakia, *Electromagnetic Surface Waves: A Modern Perspective* (Elsevier, Waltham, MA, 2013).
- ¹⁰M. G. Moharam, E. B. Grann, and D. A. Pommet, *J. Opt. Soc. Am. A* **12**, 1068 (1995).
- ¹¹M. Faryad and A. Lakhtakia, *Phys. Rev. A* **84**, 033852 (2011).
- ¹²P. Monk, *Finite Element Methods for Maxwell's Equations* (Oxford University Press, Oxford, 2003).
- ¹³R. Storn and K. Price, *J. Global Optim.* **11**, 341 (1997).
- ¹⁴M. Solano, M. Faryad, A. S. Hall, T. E. Mallouk, P. B. Monk, and A. Lakhtakia, *Appl. Opt.* **52**, 966 (2013).
- ¹⁵M. Faryad and A. Lakhtakia, *J. Nanophoton.* **6**, 061701 (2012).
- ¹⁶N. S. Kapany and J. J. Burke, *Optical Waveguides* (Academic Press, New York, NY, 1972).
- ¹⁷J. Zhang, L. Zhang, and W. Xu, *J. Phys. D: Appl. Phys.* **45**, 113001 (2012).